MATERIALS FORUM VOLUME 30 - 2006
Edited by R. Wuhrer and M. Cortie

STRUCTURAL INTEGRITY VERIFICATION OF A PRIMARY CIRCUIT PUMP FLYWHEEL FOR A NUCLEAR RESEARCH REACTOR

D. G. Carr, R. P. Harrison and W. Payten

Australian Nuclear Science and Technology Organisation,
Private Mail Bag 1, Menai, NSW, 2234, Australia

ABSTRACT

The flywheels on nuclear reactor coolant pump motors provide inertia to ensure a slow decrease in coolant flow in the event of loss of power; thus preventing possible fuel damage due to the reduced coolant flow. During operation at normal speed, a flywheel has sufficient kinetic energy to produce high-energy missiles and excessive vibration of the coolant pump assembly if the flywheel should fail. It is thus important to evaluate the fracture properties of the material to ensure it can withstand the applied stress.

The structural integrity of a large steel flywheel to be used in the primary cooling system of the OPAL research reactor at Lucas Heights was evaluated according to the requirements of the US Nuclear Regulatory Commission guide RG 1.14. The guide was developed for nuclear power plants where significant over-speeds in pumps are possible. In the OPAL reactor at ANSTO such pump over-speeds are not possible, however, the code was used to demonstrate the incredibility of failure of the flywheel. An experimental program determined the fracture toughness and tensile properties of the flywheel material; thick section AS 3678 Grade 350 plate. Revision 4 of the well-validated British Energy R6 defect assessment procedure was used to analyse the critical speed and crack length for the flywheel using the two-component failure assessment diagram which considers brittle fracture and plastic collapse. The results of the evaluation are presented in this paper, and illustrate what can be accomplished through the application of modern methods of integrity assessment.

1. INTRODUCTION

The primary cooling system (PCS) pump flywheel to be employed at the OPAL reactor consists of a 94mm thick disk, 973 mm in diameter, close-fit to a 75 mm shaft, by which torque is applied via a mechanical keyway (Figure 1). The flywheel operates in a closely controlled environment at a rated speed of 1485 rpm. Temperature and vibration sensors mounted at the PCS pump flywheel bearings provide a means of detecting abnormal operational conditions. A summary of the flywheel evaluation and the supporting test program is given in this paper.

2. EXPERIMENTAL

2.1 Materials selection

The reactor designer has selected carbon steel plate AS/NZ 3678 grade 350 for manufacture of the primary cooling system flywheels. The plate was supplied by NKK in the hot-rolled condition, the plate having an area of 2000 x 2400mm and being 100mm thick. The flywheel blanks were cut and machined from the plate and subjected to a 100% volumetric ultrasonic inspection. The flywheel was determined to be free of defects or laminations, complying with the relevant code-based acceptance criteria.

The remaining off-cuts from the plate were available for accurate material property determination of the flywheel for the purposes of the current failure assessment. The specified chemical composition of AS 3678-GR 350 steel plate to which the flywheel complied is shown in Figure 1. **Schematic of the primary cooling system reactor flywheel (not to scale).**

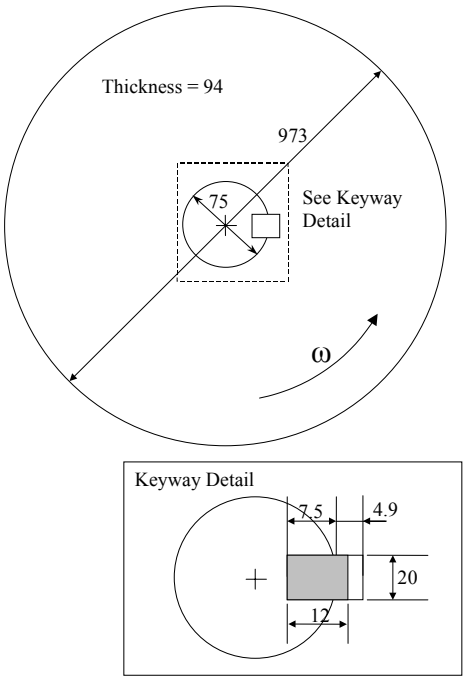

Figure 1. Schematic of the primary cooling system reactor flywheel (not to scale).

Table 1. Chemical composition of AS 3678-GR 350

Element	wt %
C	0.22 max
Si	0.55 max
Mn	1.70 max
P	0.040 max
S	0.030 max
Cr	0.30 max
Ni	0.50 max
Cu	0.40 max
Mo	0.35 max
Al	0.100 max
Ti	0.040 max
Micro-alloying elements	Nb + V: 0.030% max
C.E.	0.48 max

2.2 Tensile property determination

To account for any variation in properties through the primary cooling system flywheel, tensile tests were performed (at a constant strain rate of 8 x 10^{-5} s^{-1}) in compliance with AS 1391-1991 on cylindrical specimens sampled from varying depths in the plate [1]. Tests were performed from a set of three specimens in both the longitudinal and transverse rolling directions.

2.3 Fracture toughness - Charpy impact

Charpy impact energies where measured in the L-T and T-L orientations in accordance with AS 1544 [2]. A total of 36 standard, 10 mm thick specimens where precision electro-discharge machined (EDM) and tested in the temperature range –80 to 100°C in each of the respective orientations.

To investigate any variation in impact toughness throughout the thickness of the flywheel, a set of 9 specimens were tested through the plate depth at a temperature close to the flywheel operating temperature (~20°C).

2.4 Fracture toughness – J_{Ic}

Precise measurement of the primary cooling system flywheel fracture toughness poses challenges because of the large material volume required to meet the "validity" requirements of testing standards and the limited flywheel material available. Five, T-L and L-T, three-point bend specimens (SE(B)) were EDM machined with dimensions 40 x 30 mm for the width and breadth respectively. The specimens had a span-to-width ratio of 4 and were pre-fatigued at room temperature on a servo-hydraulic test machine. They were subsequently side-grooved to produce sharp, straight crack fronts with a crack depth a/W ratio of 0.5. Testing was performed in a liquid nitrogen cooled environmental chamber, on an electro-mechanical universal test machine. The test temperature was selected to be as close as practically possible to the estimated 100 MPa√m transition temperature, according to the guidance of ASTM E 1921-02 *Standard Test Method for Determination of Reference Temperature, To, for Ferritic Steels in the Transition Range* [3]. An acoustic emission sensor was mounted on the sample to aid in the determination of the onset of slow stable crack propagation.

The ASTM standard E1921-02 [3] imposes the requirement that cleavage fracture toughness data should satisfy the conditions of small scale yielding. This can be assessed by comparing the measured K_{Jc} values with the specimen capacity limit expressed as:

$$K_{Jc(limit)} = \sqrt{\frac{Eb_o\sigma_{ys}}{30(1-\nu^2)}} \qquad (1)$$

where, E = Young's Modulus; b_o = remaining ligament; σ_{ys} = material yield strength at the test temperature; and ν = Poisson's ratio. Measured values of K_{Jc} in excess of the estimated specimen capacity were treated as censored values of toughness equal to $K_{Jc(limit)}$. Censored values contained statistically useful information used in the analysis of the data.

The material yield strength at the test temperature was estimated from the load/crack opening displacement (COD) curve using the plane strain Tresca solution for the test geometry [4]:

$$n_L = \frac{2SN_L}{W^2 t\sigma_y} \qquad (2)$$

Where n_L=1.22(1- a/W)^2; t=30mm and N_L is the limiting load at the departure from elastic behaviour on the load versus displacement curve.

The J-integral was determined from the experimental load-COD record using,

$$J = \frac{K^2\left(1-\nu^2\right)}{E} + \eta^{COD}\frac{U_p^{COD}}{b_o B_N} \qquad (3)$$

In Eq. 3, K denotes the linear stress intensity factor; U^{COD} denotes the plastic area under the load-COD curve; and η^{COD} is a dimensionless parameter that relates plastic work done on the specimen to crack growth resistance based on the load-COD record. Yun-Jae Kim, et al. have recently shown that experimental J estimation based on the COD is almost insensitive to B/W and strain hardening, regardless of a/W [5]. For the current work, η^{COD} was defined by [5]:

$$\eta^{COD} = 3.724 - 2.24\left(\frac{a}{W}\right) + 0.408\left(\frac{a}{W}\right)^2 \qquad (4)$$

$$\text{for} \qquad 0.1 \le a/W \le 0.7$$

The fracture toughness K_{Jc} of the specimens was determined for each datum J at the onset of cleavage (initiation) fracture, J_c using the plane strain condition:

$$K_{Jc} = \sqrt{J_c \frac{E}{1-\nu^2}} \qquad (5)$$

Charpy results indicate that the primary cooling pump flywheel exhibits brittle transition behaviour. For steels exhibiting such behaviour the master curve approach has been widely adopted as a method for determining fracture toughness as a function of material thickness and temperature [3;6-9]. The basis of the master curve approach is a three-parameter Weibull model to define the relationship between K_{Jc} and the cumulative probability for failure,

$$p_f = 1 - \exp\left[-\left(\frac{K_I - K_{min}}{K_o - K_{min}}\right)^4\right] \qquad (6)$$

where P_f is the cumulative probability for failure, K_I the fracture toughness of the material, K_{min} the theoretical lower bound fracture toughness set at 20 MPa√m, and K_o the Weibull scale parameter. The slope parameter used is 4, describing the theoretical and observed scatter for a homogenous ferritic steel [10].

The experimental results were conservatively fitted to this model taking into account the possibility of material inhomogeneity and making adjustment for the small test population size. This was achieved by means of the three-step SINTAP assessment procedure using the maximum likelihood method (MML) [11]. The first step yielded the median value of fracture toughness. Stage 2 involved performing a lower tail MML estimation, checking and correcting any undue influence of excessive values in the upper tail distribution. Stage 3 was used to determine a minimum value estimation to yield the characteristic toughness of the material. The SINTAP procedure is outlined in detail in reference 9.

2.5 Failure analysis – R6 assessment

Failure analysis called for in nuclear codes, and any other failure assessment, must be based on appropriate conservative assumptions for stress level, flaw size, temperature, and fracture toughness. The methodology of the R6 nuclear code, *Assessment of the integrity of structures containing defects* procedure was used to evaluate the primary cooling system flywheel [12]. The R6 procedure is well established, has been rigorously verified, and forms the basis for other failure assessment guides such as BS7910 [13-18].

In this case two flywheel failure modes are assessed: plastic collapse and initiation of brittle fracture. Plastic collapse is controlled by overall plasticity in the defective section and the local crack-tip stress-strain fields control the initiation of fracture. The basic approach used in R6 for the assessment consists of evaluating parameters K_r and L_r, dependent on the applied loads, material properties, and geometry including defect size and shape. K_r and L_r are defined in this case by

$$K_r = \frac{K}{K_{mat}}, \qquad (7)$$

$$L_r = \frac{P}{P_L(\sigma_y)}, \qquad (8)$$

where K is the stress intensity factor at load P, P_L is the cracked-body rigid-plastic limit load for a flow stress equal to the material's 0.2% proof stress, σ_y, and K_{mat} is the fracture toughness. The assessment point (L_r, K_r) is plotted on the failure assessment diagram (FAD), and compared with the bounding curve defined by $K_r = f(L_r)$. If the assessment point lies within the curve "failure" is avoided. If the point lies outside the curve, then the failure avoidance criterion was violated. In this case, the Option 2 bounding curve is used to provide a conservative failure criterion taking into account the material specific behaviour derived from the experimental stress-strain data.

The R6 analysis discussed in detail below involves two parts: the calculation of the critical crack length when operating at 125% of the primary cooling system flywheel design speed (that is, at 1856 rpm); and the calculation of the critical over-speed for the minimum detectable flaw.

3. RESULTS AND FAILURE ANALYSIS

3.1 Tensile properties

The tensile properties of the flywheel material were relatively similar in both the longitudinal and transverse directions. Discontinuous yielding was observed for all but one longitudinal specimen, which exhibited continuous yielding and a measured 0.2% proof stress of 349 MPa. The mean tensile properties to one standard sample deviation are summarised in Table 2. These compared favourably with the minimum specified properties of AS 3678 grade 350 plate. Use of the stress-strain curves enabled calculation of the option 2 FAD. However, the material properties from the tensile tests should be conservatively considered as estimate values only. Therefore, the lower bound estimate of yield and UTS used in the assessment of the component was the specified minimum requirement of AS 3678, grade 350 steel (Table 2).

Table 2. Tensile properties of the OPAL reactor flywheel material and AS 3678-350 minimum requirements.

	E [GPa]	YS [MPa]	UTS [MPa]	%RA
Longitudinal	207±5	352±2*	538±2	77±1
Transverse	212±5	351±9	535±2	78±2
Minimum Requirement	-	330	450	-

* mean and s.d. of two specimens exhibiting discontinuous yielding.

3.2 Flywheel fracture toughness

The Charpy results shown in Figure 2 indicate the T-L orientation of the plate exhibits transitional behaviour at the flywheel operating temperature of 20°C. Thus, it can be said that toughness decreases with increasing thickness, as the probability of brittle initiator in the stress field around the crack tip increases. Consequently, the use of the statistical model of Eq. 6 was necessitated to account for the effects of flywheel thickness relative to the test specimen and of temperature. These results indicate that cracks propagating in the T-L plate orientation are more probable than in the L-T direction where the recorded Charpy impact energies are higher.

The Charpy results also indicated a decrease in the absorbed energy at the centre of the plate of about 100 J, in the T-L orientation, where banding and segregation effects are likely to be most severe. The effect of this apparent inhomogeneity had a minor effect according to the SINTAP minimum value estimate analysis of the data and was within the bounds of normal transitional behaviour scatter. The uncertainty in values of K_{mat} associated with the small number of valid test results was corrected for using this method by a right-shift in the 100 MPa√m reference temperature. The lower 2% confidence curve for the J-integral tests is shown in Figure 3, two points are in excess of the specimen capacity defined in Eq. 1 and exhibited greater than 1 mm of slow stable crack growth prior to cleavage fracture. These were treated as censored values in the MML estimate. The minimum value estimate curve in Figure 3 is compared with a lower bound Charpy correlation provided in BS7910:1999 *Guide on methods for assessing the acceptability of flaws in metallic structures*.

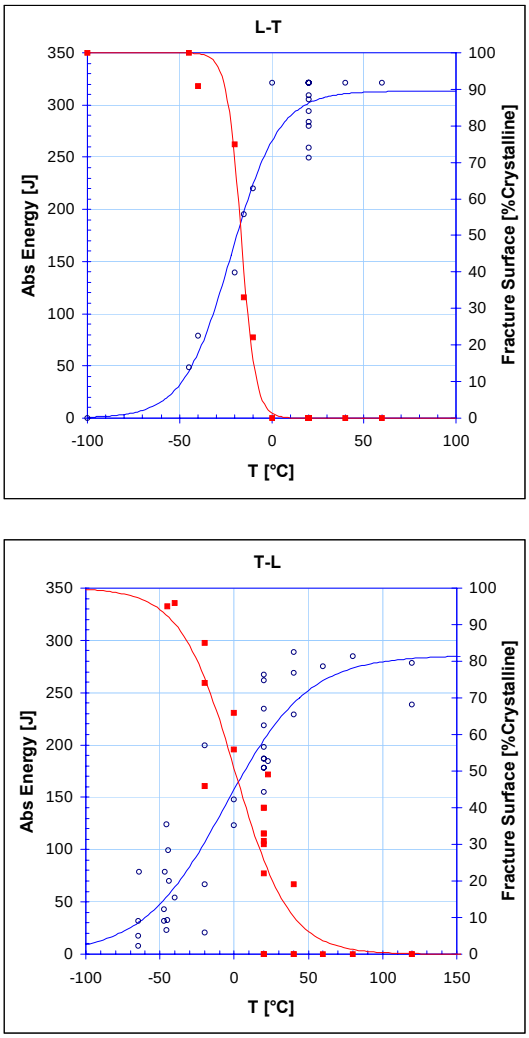

Figure 2. Charpy impact energy toughness for the plate orientations L-T and T-L. Note the brittle transition behaviour in the T-L direction at 20 °C. A defect is most likely to propagate in the T-L direction.

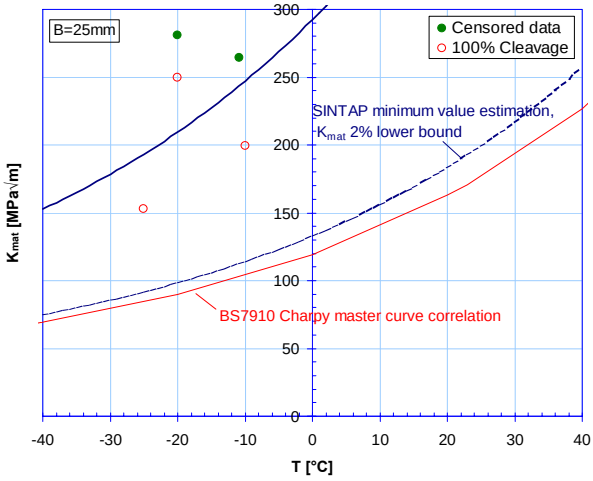

Figure 3. Estimated flywheel toughness derived from Charpy and K_{Jc} data.

The Charpy correlation with fracture toughness can be approximated by the master curve as follows [19]:

$$K_{mat} = 630 + [350 + 2435 \exp\{0.019 (T - T_{27} - 3)\}](25/B)^{1/4} [\ln\{1/(1-P_f)\}]^{1/4} \quad (9)$$

Where,

K_{mat}	is in N/mm$^{3/2}$
T	is the temperature at which K_{mat} is to be determined (°C)
T_{27J}	is the 27 J Charpy transition temperature (°C)
B	is the thickness of the material (94 mm in the case of the flywheel)
P_f	is the probability of failure taken in this case at 5%.

The validity of the BS7910 Charpy correlation defined in Eq. 9 for pressure vessel-type steels and thin high strength steels has been established [20]. Further examples of its application have been demonstrated with data sets from parent plates, sections, pipeline, weld metals and HAZs. This curve also compared favourably with the J-integral results attained, and in order to manifest a conservative approach, the primary cooling system flywheel toughness was estimated using this lower bound correlation, justified by the experimental evidence. Incorporating the 36 Charpy data points for the T-L orientation, K_{mat} was estimated to be 91 MPa√m for the flywheel thickness of 94 mm at the lowest foreseeable operating temperature of 0°C.

3.3 Loading

The stresses in the primary cooling system pump flywheel, neglecting local stress concentrations such as keyways, can be calculated by the following plane stress equations [21],

$$\sigma_r = \left(\frac{3+\nu}{8}\right)\rho\omega^2\left[R_o^2 + R_i^2 - \frac{R_i^2 b^2}{r^2} - r^2\right] \quad (10)$$

and

$$\sigma_\theta = \left(\frac{3+\nu}{8}\right)\rho\omega^2\left[R_o^2 + R_i^2 - \frac{R_i^2 R_o^2}{r^2} - \left(\frac{1+3\nu}{3+\nu}\right)r^2\right] \quad (11)$$

where R_i and R_o are the inner and outer radius respectively, ω is the angular velocity defined in Figure 1. Substituting the appropriate geometric data from the PCS pump flywheel, centrifugal stresses were calculated at an over-design speed of 125% corresponding to an angular velocity of 194 rad.s^{-1}, with the material density ρ given by 7801 kg/m^3.

The stresses for the appropriate flywheel geometry are shown in Figure 4. Note that the stresses are at a maximum in the hoop direction, particularly at small radii due to the stress concentration effect of the bore. Although the magnitude of the stress varies with angular velocity, the profile of the stress distribution of Figure 4 remains the same. The maximum tensile stress at any point in the flywheel is equal to the hoop stress.

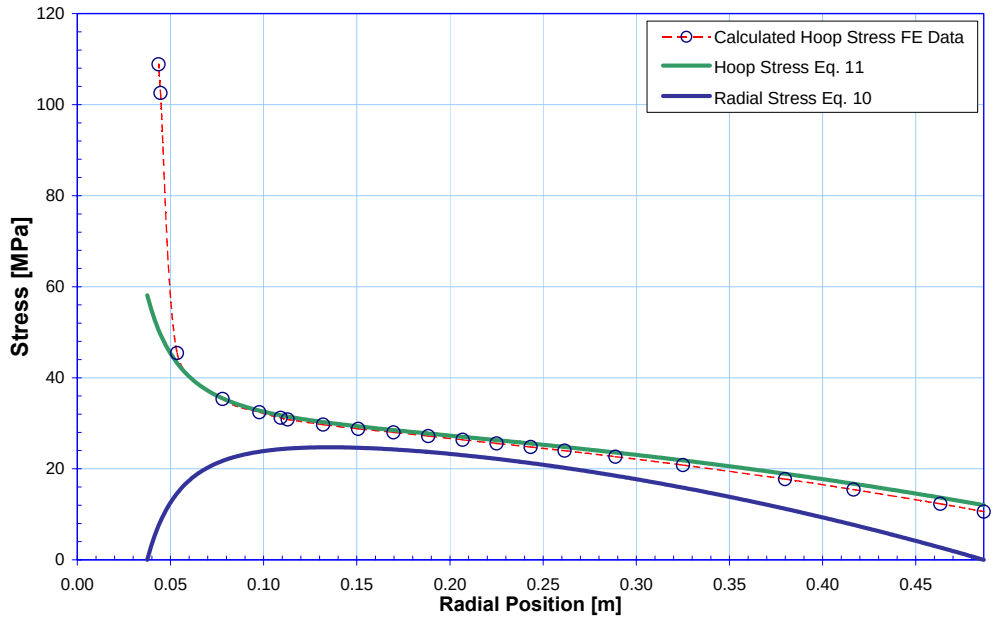

Figure 4. Shape of the flywheel stress distribution at 194 rad.s^{-1}.

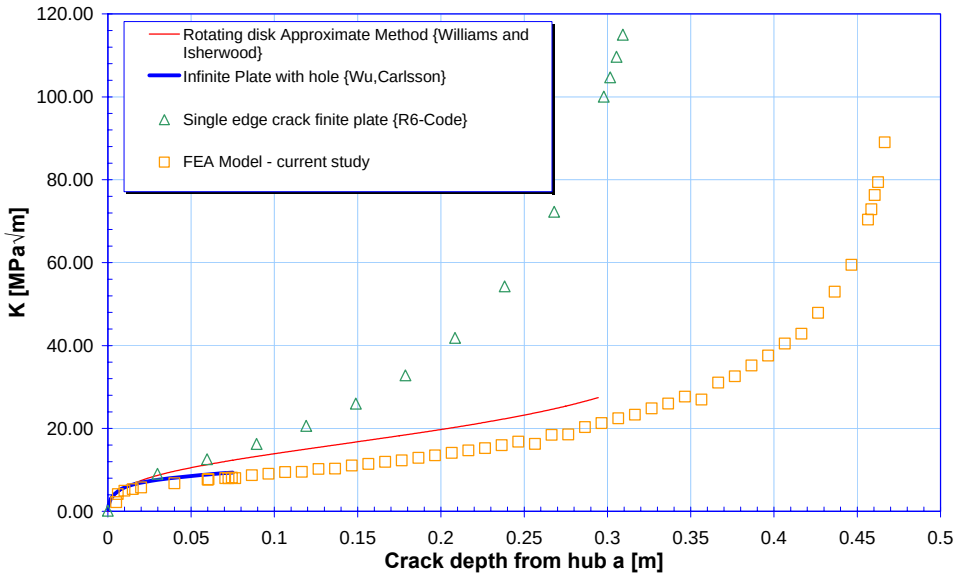

Figure 5. Stress intensity factor computations for the reactor primary cooling system flywheel at an angular velocity of 157 rad.s^{-1}.

Other stresses acting on the flywheel must also be taken into consideration. The PCS pump flywheel operates within a narrow range of controlled temperature and thus thermal stresses were neglected in the calculation.

Start-up stresses were also analysed to determine the worst case conditions. The maximum torque applied through the pump shaft at start-up was 1273 Nm, which corresponded to a maximum force of 33953 N, or 77 MPa over the key contact area.

Tolerances on the dimensions for the keyway allow for an interference of 0.026 mm. This was also considered in the fracture analysis, having a negligible long-range effect on the overall stress distribution; this being dominated by the centrifugal stresses.

3.4 Flaw geometry

The worst-case defect, as shown by the material properties and stress analysis, was modelled as a through-thickness flaw emanating from the corner of the keyway in the T-L plate orientation.

3.5 Stress intensity factor

A stress intensity factor (SIF) solution for a through-thickness crack emanating from the corner of the keyway was determined by finite element analysis. The SIF was modelled using the FRANC2D (FRacture Analysis Code) computer program, freely available from the Cornell Fracture Group at Cornell University. FRANC2D is a two dimensional, finite element based program for simulating curvilinear crack propagation in planar (plane stress, plane strain, and axisymmetric).

The crack was simulated using a rosette of quarter-point, six-node triangular elements around the crack tip to model the inverse square-root stress singularity. Stress intensity factors were calculated using the displacement correlation method. The crack propagation path from the corner of the keyway was determined from the predicted crack propagation angle using the maximum tangential stress theory. This was achieved by small increments of crack length from the keyway corner towards the outer boundary of the flywheel, yielding the crack propagation path and the corresponding SIF. The flywheel was modelled assuming symmetry along the midpoint of the keyway, under plane stress conditions, the results of which are shown in Figure 5. The SIF is in close agreement with that for a radial crack at a circular hole in an infinite plate reported by Wu and Carlson [22], which is valid for short crack lengths well below the estimated critical crack size. The modelled SIF also shows the approximate solution of Williams and Isherwood to be overly conservative for a radial crack emanating from the bore of a rotating disk (no keyway) [23].

The SIFs arising from the design allowable interference between the key and keyway hub, as well as the SIF arising from start-up stresses via the pump torque distributed over the bearing area of the key, were calculated in a similar manner. Both SIF's diminished to less than 1 MPa√m at a crack length of over 0.07 m and did not contribute significantly to the total SIF or failure of the component.

The SIF's, calculated as a function of angular velocity and crack length, were used to determine the R6 parameter K_r as follows:

$$K_r = \frac{K_I^p(a)}{K_{mat}} + \frac{K_I^s(a)}{K_{mat}} = \frac{f\omega^2\sqrt{\pi a}}{K_{mat}} + \frac{K_I^{int}(a)}{K_{mat}} + \rho(a) \qquad (12)$$

where,

$K_I^p(a)$ = the linear elastic stress intensity factor for the flaw size a, for the loads giving rise to primary stresses as defined by the R6 procedure [12].

$K_I^s(a)$ = the linear elastic stress intensity factor for the flaw size a, for the loads giving rise to secondary stresses such as those due to interference at the keyway $K_I^{int}(a)$.

f = a function incorporating the geometry and material properties of the flywheel, determined from the FE model.

ω = the angular velocity of the flywheel

ρ = a plasticity correction factor as a function of flaw size a, that takes into account interactions between secondary and primary stresses.

3.6 Limit load solution

The limit load solution required in Eq. 8 was taken from [12] for an extended defect in a plate under combined tension and bending. The modified limit load solution for an extended defect in the primary cooling system flywheel under combined tension and bending can be defined as:

$$N_L = 2t(R_o - R_i)\sigma_y \left[\frac{(1-\alpha)^2}{2\lambda + \alpha + \sqrt{(2\lambda+\alpha)^2 + (1-\alpha)^2}} \right] \qquad (13)$$

where t is the thickness of the flywheel; R_o is the outer radius; R_i is the inner radius defined at the outer corner of the keyway; σ_y is the yield stress; α is the ratio of crack length to the distance (R_o-R_i); and $\lambda = 1/6(\sigma_b/\sigma_m)$, a ratio of bend to membrane stress. In order to apply the limit load of Eq. 13 to the non-linear stress profile shown in Figure 4 the principal stress must be resolved into it's membrane and bending components

$$P_m = \frac{1}{(R_o - R_i)} \int_{R_i}^{R_o} \sigma dr \qquad (14)$$

$$P_b = \frac{6}{(R_o - R_i)^2} \int_{R_i}^{R_o} \sigma(r_m - r) dr \qquad (15)$$

where r_m is the flywheel mean radius. Substitution of the appropriate geometric data and stress enabled calculation of L_r and determination of the assessment point location on the failure assessment diagram for a given flaw length and angular velocity.

4. DISCUSSION

The R6 calculations have been performed following the procedure outlined in Section 2 and the assessment points have been compared with the R6 Option 2 curve [12]. Results are shown in Figure 6 for increasing crack depths at the 125% speed and in Figure 7 as a function of angular velocity for a large assumed defect of 100 mm which has escaped detection. In reality the maximum expected size flaw that could escape detection is much smaller.

It is apparent from Figure 6 that at the 125% over-speed, failure tends towards plastic collapse and that L_r is weakly dependant on crack length. Failure is indicated at a crack length of 355 mm, indicating that

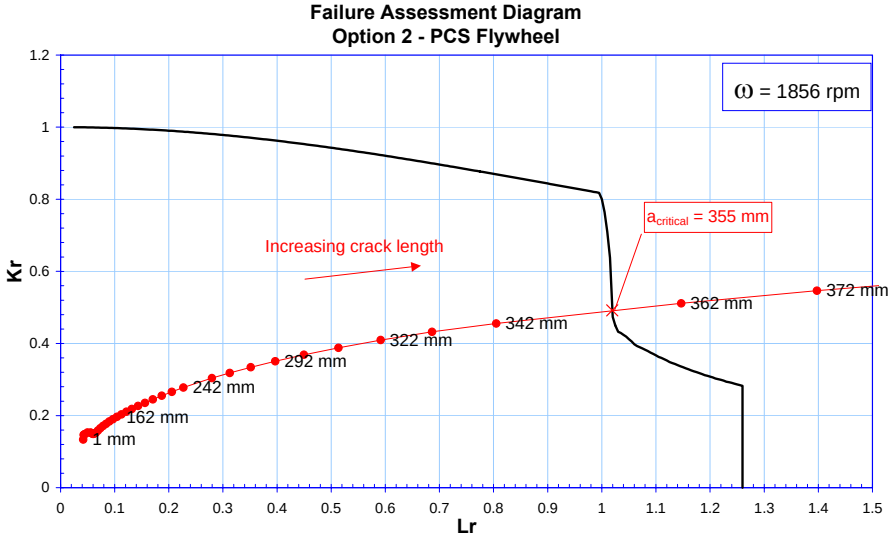

Figure 6. Loci of assessment points on the failure assessment diagram as a function of crack depth, at 125% primary cooling system pump flywheel over-speed.

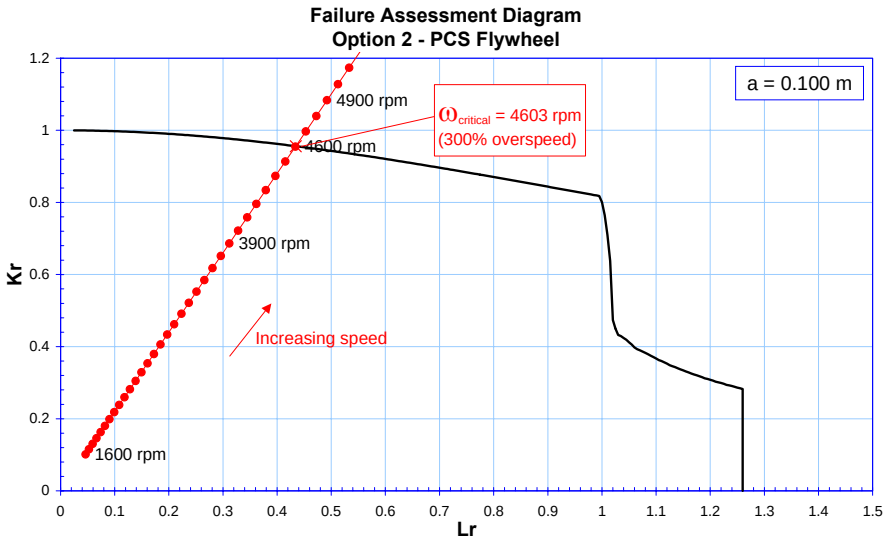

Figure 7. Loci of assessment points as a function of angular velocity for a 100mm deep defect emanating from the PCS pump flywheel keyway corner.

the PCS flywheel is extremely tolerance to such defects. This may be expected from Figure 4 as the principal stress decreases radially in the uncracked component. Conversely, the SIF increases gradually, then rapidly as the outer boundary is approached. In the cracked component, the elastic stresses are readily constrained by the surrounding material almost until crack length is at break-through at the outer boundary.

While the K_{mat} of 91 MPa√m used in the assessment is believed to be conservative, it can be demonstrated that the assessed condition of the flywheel is not sensitive to variation in toughness. A sensitivity study performed on variations in flywheel fracture toughness is shown in Figure 8. The reserve on toughness is the fractional distance of an assessment point to the FAD bounding curve, along a line intersecting the origin, the assessment point and the FAD bounding curve, at a particular load condition, toughness and flaw length. It can be observed from Figure 8 that there is a safe, gradual trend towards the limiting condition and that the assessed condition is a considerable distance from the limiting toughness of 6 MPa√m for the maximum assumed flaw. This provides ample margin for error in the measured material fracture toughness. Similar margins were demonstrated for variations in material yield stress and defect length.

Although the primary cooling system flywheel is likely to fail by a plastic collapse mechanism at 125% over-speed, subsequent increases in angular velocity move the problem more towards brittle fracture. This is apparent from the results presented in Figure 7 for the limiting over-speed condition. The accuracy of the limit load solution becomes less important in this case and for a crack length of 100mm, failure is indicated at an over-speed of 300%. Overall, it is shown that the load carrying capacity of this component is little affected by the presence of defects of this size.

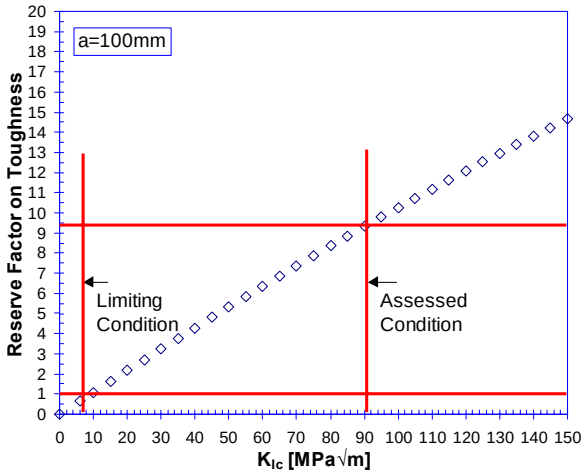

Figure 8 A sensitivity study on the primary cooling system flywheel toughness at 125% over-speed.

5. CONCLUSIONS

A detailed evaluation has been performed to determine the critical speed for the primary cooling system pump flywheel from the standpoint of fracture and subsequent missile production. The incredibility of failure by plastic collapse and brittle fracture has been demonstrated using the R6 methodology and utilising conservative estimations of tensile and fracture properties. The over-speed necessary for failure is in excess of 300% of the design speed. At 125% over-speed the primary cooling system pump flywheel is relatively insensitive to a defects emanating from the keyway corner. The critical crack length under these conditions is 355 mm.

Acknowledgements

The authors wish to gratefully acknowledge the experimental assistance of T. Nichols, J. Merhebi and G. Atkinson.

References

1. Australian Standard 1391, *Methods for tensile testing of metals*, AS1391, SAI Global, 1991.
2. Australian Standard 1544, *Impact tests on metals*, AS1544, SAI Global, 2003.
3. ASTM International E1921, *Standard Test Method for Determination of Reference Temperature, To for Ferritic Steels in the Transition Range*, E1921, ASTM, 2002.
4. A.G. Miller, *Review of limit loads of structures containing defects*, Int. J. Pres. Ves. Pip., 1988, vol. 32, pp. 197-327.
5. Yun-Jae Kim, Jin-Su Kim, Soo-Man Cho, and Young-Jin Kim, *3-D constraint effects on J testing and crack tip constraint in M(T), SE(B), SE(T) and C(T) specimens: numerical study*, Eng. Fract. Mech., 2004, vol. 71, pp. 1203-18.
6. G. Nagel, and J.-G. Blauel, *Evaluation of the standard master curve for fracture toughness determination*, Nucl. Eng. Des., 1998, vol. 190, pp. 159-69.
7. K. Wallin, P. Nevasmaa, A. Laukkanen, and T. Planman. *Master Curve analysis of inhomogeneous ferritic steels,* Eng. Fract. Mech., 2004, vol. 71(16-17), pp. 2329-2346.
8. D.E. McCabe, J.G. Merkle, and K. Wallin. *Technical basis for the master curve concept of fracture toughness evaluations in the transition range*, ASTM Special Technical Publication [1360], ASTM, Philadelphia, PA, 1999, pp. 21-33.
9. IAEA, *Guidelines for Application of the Master Curve Approach to Reactor Pressure Vessel Integrity in Nuclear Power Plants*, Technical Reports Series, IAEA, Vienna, 2005, no. 429.
10. K. Wallin, *The Scatter in KIc-Results*, Eng. Fract. Mech., 1984, vol. 19, pp. 1085-93.
11. British Steel, *SINTAP - Structural Integrity Assessment Procedures for European Industry*, Project BE95-1426, Final Procedure, internal report, British Steel, Rotherham, 1999.
12. R6, *Assessment of the integrity of structures containing defects*, Revision 4, British Energy Generation Ltd., Gloucester, 2004.
13. R.A. Ainsworth, A.R. Dowling, I. Milne, and A.T. Stewart, *Revision 3 Of R6, Its Background And Validity*. ECF 6: Fracture Control of Engineering Structures, Proceedings of the 6th Biennial European Conference on Fracture, Engineering Materials Advisory Services Ltd., Warley, 1986.
14. I. Milne, R.A. Ainsworth, A.R. Dowling, and A.T. Stewart, *Assessment Of The Integrity Of Structures Containing Defects*, Int. J. Pres. Ves. Pip., 1988, vol. 32(1-4), pp. 3-104.
15. D. Green, B.D. Daniels, and R.A. Ainsworth, *Application of the R6 Failure Assessment Diagram to UK nuclear plant assessments*, American Society of Mechanical Engineers, Pressure Vessels and Piping Division, PVP. Vol. 323(1)., New York, 1996.
16. I. Milne, R.A. Ainsworth, A.R. Dowling, and A.T. Stewart, *Background to and Validation of CEGB Report R/H/R6 - Revision 3*. Int. J. Pres. Ves. Pip., 1988, vol. 32(1-4), pp. 105-196.
17. U. Zerbst, R.A. Ainsworth, and K.-H. Schwalbe, *Basic principles of analytical flaw assessment methods*, Int. J. Pres. Ves. Pip. 2000, vol. 77(14-15), pp. 855-867.
18. P. J. Budden, J.K. Sharples, and A.R. Dowling, *The R6 procedure: recent developments and comparison with alternative approaches*, Int. J. Pres. Ves. Pip., 2000, vol. 77(14-15), pp. 895-903.
19. British Standards 7910. *Guide on methods for assessing the acceptability of flaws in metallic structures*, Incorporating Amendment 1, BS7910, BSI, 1999.
20. A.C. Bannister, *Determination of fracture toughness from Charpy impact energy: procedure and validation*, British Steel, Swindon Technology Centre, 1998.
21. S. Timoshenko and J.N. Goodlier, *Theory of Elasticity*, 3rd Edition, McGraw-Hill Kogakusha Ltd, Tokyo, 1970.
22. Xue-Ren Wu and Carlsson A.J., Weight Functions and Stress Intensity Factor Solutions, 1st Edition, Pergamon Press, Oxford, New York, 1991.
23. J.G. Williams and D.P. Isherwood, *Calculation of the Strain-Energy Release Rates of Cracked Plates by an Approximate Method*, Journal of Strain Analysis, 1968, vol. 3, pp. 17-22.